Inorg. Chem. **2006**, *45*, 7339–7347

Dual Fluorescence from an *Isonido* Re^{III} Rhenacarborane Phosphine Complex, [7,10-μ-H-7-CO-7,7-$(PPh_3)_2$-*isonido*-7,8,9-$ReC_2B_7H_9$]

Steven W. Buckner,[†] Matthew J. Fischer,[†] Paul A. Jelliss,*[,†] Rensheng Luo,[‡] Shelley D. Minteer,[†] Nigam P. Rath,[‡] and Aleksander Siemiarczuk[§]

Department of Chemistry, Saint Louis University, St. Louis, Missouri 63103, Department of Chemistry and Biochemistry, University of Missouri−St. Louis, St. Louis, Missouri 63128, and Fast Kinetics Application Laboratory, Photon Technology International (Canada), Inc., 347 Consortium Court, London, Ontario, Canada N6E 2S8

Received June 14, 2006

The complex [7,10-μ-H-7-CO-7,7-$(PPh_3)_2$-*isonido*-7,8,9-$ReC_2B_7H_9$] has been synthesized by treatment of the complex salt $[NHMe_3][3,3\text{-}Cl_2\text{-}3,3\text{-}(CO)_2\text{-}closo\text{-}3,1,2\text{-}ReC_2B_9H_{11}]$ with PPh_3 in refluxing THF (tetrahydrofuran) and isolated as intensely colored orange-red microcrystals. Spectroscopic NMR and IR data have suggested that the product has a highly asymmetric structure with two inequivalent PPh_3 ligands and a single CO ligand. Measurement of ^{11}B NMR spectra in particular have indicated seven distinct boron vertexes, although the resulting cage degradation by removal of two BH vertexes was confirmed only following X-ray crystallographic analysis, which revealed the pentadecahedral *isonido*-7,8,9-ReC_2B_7 architecture. The ^{11}B NMR resonances span an enormous chemical shift range ($\Delta\delta = 113$), and this appears to be a direct consequence of the deshielding of the boron vertex directly opposite the quadrilateral $\overline{ReCCB}$ aperture. The new complex has been shown by electrochemical measurements to undergo a reversible one-electron oxidation. Digitally simulated cyclic voltammograms support a proposed square scheme ($E_{1/2} = 0.58$, 0.69 V vs ferrocene) involving a reversible *isonido–closo* transition of the metallacarborane cage. Most unusually for a metallacarborane complex, ambient temperature solutions in CH_2Cl_2 and DMF have been shown to be intensely turquoise-blue fluorescent ($\lambda_{em} = 442$ nm, $\Phi = 0.012$). Fluorescence spectroscopy measurements in MeTHF (2-methyltetrahydrofuran) glass at 77 K have indicated that the likely cause of such a broad emission is dual fluorescence ($\lambda_{em} = 404$, 505 nm), with both emissions displaying vibronic structure. Following excited-state lifetime decay analysis, the emissive behavior has been accredited to metal-perturbed ^{1}IL states, with the lower energy emission arising from a slight geometric distortion of the initially excited complex.

Introduction

For 40 or so years, it has been known that carborane cages can mimic cyclopentadienide ligands in their haptotropic binding to d-block metal−ligand fragments.[1] From the perspective of the boron chemist, the metal−ligand moiety is merely an isolobal replacement for the simple BH vertex.[2] Irrespective of one's viewpoint, an expanding array of aesthetically fascinating metallacarborane structures have been discovered and rationalized (in most cases) using the Wade−Williams protocol for cage-cluster counting.[3] We report herein a novel *isonido*-ReC_2B_7 complex, which exhibits exceptional optoelectronic properties for this class of complex. While a range of sandwich and half-sandwich MC_2B_9 metallacarboranes have been electrochemically analyzed,[4] reports of luminescence from metallacarborane complexes are few and far between.[5] Our own efforts in this

* To whom correspondence should be addressed. E-mail: jellissp@slu.edu.
† Saint Louis University.
‡ University of Missouri−St. Louis.
§ Photon Technology International, Inc.

(1) (a) Hosmane, N. S. *Pure Appl. Chem.* **2003**, *75*, 1219. (b) Grimes, R. N. *Coord. Chem. Rev.* **2000**, *200−202*, 773. (c) Grimes, R. In *Comprehensive Organometallic Chemistry II*; Abel, E. W., Stone, F. G. A., Wilkinson, G., Eds.; Pergamon Press: Oxford, UK, 1995; Vol. 1, Chapter 9. (d) Callahan, K. P.; Hawthorne, M. F. *Adv. Organomet. Chem.* **1976**, *14*, 145. (e) Hawthorne, M. F. *Pure Appl. Chem.* **1973**, *39*, 475. (f) Hawthorne, M. F.; Young, D. C.; Andrews, T. D.; Howe, D. V.; Pilling, R. L.; Pitts, A. D.; Reintjes, M.; Warren, L. F., Jr.; Wegner, P. A. *J. Am. Chem. Soc.* **1968**, *90*, 879.

(2) O'Neill, M. E.; Wade, K. In *Comprehensive Organometallic Chemistry*; Wilkinson, G., Abel, E. W., Stone, F. G. A., Eds.; Pergamon Press: Oxford, UK, 1982; Vol. 1, Section 1.

(3) (a) Wade, K. *Adv. Inorg. Chem. Radiochem.* **1976**, *18*, 1. (b) Williams, R. E. *Adv. Inorg. Chem. Radiochem.* **1976**, *18*, 67.

10.1021/ic061071n CCC: $33.50
Published on Web 08/08/2006

Scheme 1. Synthesis of [7,10-μ-H-7-CO-7,7-$(PPh_3)_2$-*isonido*-7,8,9-$ReC_2B_7H_9$] (**2**)

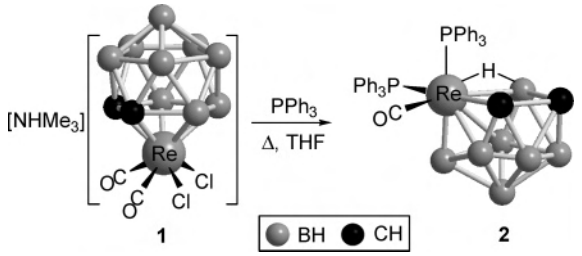

area are just beginning to yield dividends, with results so far limited to strong phosphorescence at low temperature (77 K) only.[6] We nevertheless report surprisingly strong fluorescence from the new *isonido*-ReC_2B_7 complex in solution at ambient temperatures, which, from analysis of emission characteristics and lifetimes at ambient and liquid nitrogen temperatures, appears to be anomalously bifurcated.

Results and Discussion

Treatment of the recently reported complex salt $[NHMe_3][3,3\text{-}Cl_2\text{-}3,3\text{-}(CO)_2\text{-}closo\text{-}3,1,2\text{-}ReC_2B_9H_{11}]$ (**1**)[6a] with PPh_3 in refluxing THF (tetrahydrofuran) yielded, as one of two products, the bright orange-red complex [7,10-μ-H-7-CO-7,7-$(PPh_3)_2$-*isonido*-7,8,9-$ReC_2B_7H_9$] (**2**) in low yield (Scheme 1). The second product has not been formally identified yet but is apparently formed in even lower yield.

Despite NMR and IR measurements that were straightforward in appearance, the identity of complex **2** was not formally deduced until single crystals were procured for X-ray crystallographic analysis. The structure is shown in Figure 1 along with pertinent structural parameters. Most striking is the excision of two BH vertexes from the starting material to yield a ReC_2B_7 cage system. The source of cage degradation is debatable because PPh_3 would not normally be expected to act as a potent enough base to promote deboronation. However, such a mechanism may be facilitated by the marginally elevated +3 oxidation state (vide infra) of rhenium in compound **1**. In this respect, it should be noted that our own observations of the reactivity of the Re^{III}–carborane complex $[3\text{-I-}3,3,3\text{-}(CO)_3\text{-}closo\text{-}3,1,2\text{-}ReC_2B_9H_{11}]$ revealed it to be especially susceptible to nucleophilic attack under mildly basic conditions at the β-B vertex of the

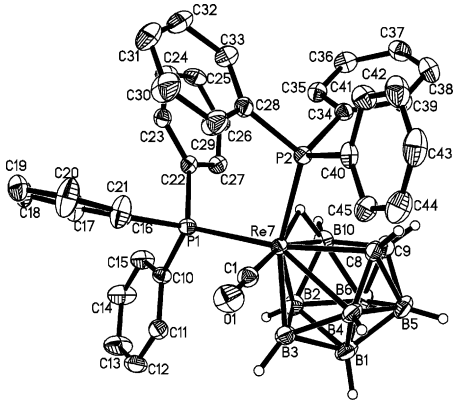

Figure 1. Molecular geometry of complex **2**. Selected bond lengths (Å) and angles (deg): Re(7)−C(1) 1.924(4), Re(7)−B(3) 2.142(5), Re(7)−C(8) 2.248(4), Re(7)−B(4) 2.357(5), Re(7)−B(2) 2.377(5), Re(7)−B(10) 2.413-(5), Re(7)−P(1) 2.4507(10), Re(7)−P(2) 2.4625(11), Re(7)−H(7) 1.69(6), C(8)−C(9) 1.522(7), B(10)−C(9) 1.659(7), C(1)−O(1) 1.156(5); C(1)−Re(7)−C(8) 109.98(18), C(1)−Re(7)−B(10) 161.82(19), C(8)−Re(7)−B(10) 63.21(17), C(1)−Re(7)−P(1) 91.67(14), B(3)−Re(7)−P(1) 102.55-(14), C(8)−Re(7)−P(1) 158.36(12), B(10)−Re(7)−P(1) 96.18(13), C(1)−Re(7)−P(2) 88.90(13), B(3)−Re(7)−P(2) 152.07(14), C(8)−Re(7)−P(2) 79.40(12), B(2)−Re(7)−P(2) 149.18(14), B(10)−Re(7)−P(2) 105.47(13), P(1)−Re(7)−P(2) 101.52(4), C(9)−B(10)−Re(7) 92.8(3), O(1)−C(1)−Re-(7) 177.6(4), C(9)−C(8)−Re(7) 103.5(3), C(8)−C(9)−B(10) 100.5(4).

coordinating CCBBB face, although deboronation was not a consequence on this occasion.[6a] The $[NHMe_3]^+$ counterion could also feasibly act as a source of the base NMe_3 under the conditions of the reaction.

The cage structure of complex **2** is not perfectly deltahedral, with an open quadrilateral face defined by the vertexes Re(7)C(8)C(9)B(10) and with the opposite corners clearly nonbonded (Re(7)−C(9) 2.994, C(8)−B(10) 2.446 Å, cf. Re-(7)−C(8) 2.248(4), C(9)−B(10) 1.659(7) Å). One of these edges, Re(7)−B(10), is bridged by an endopolyhedral proton H(7), which was located in the difference Fourier map. The asymmetry caused by this facial configuration is compounded by the orientation of the tripodal $Re(CO)(PPh_3)_2$ vertex with respect to the carborane cage. Thus one of the PPh_3 ligands is directly trans (B(3)−Re(7)−P(2) 152.07(14)°) to the boron atom B(3) of the lower pentagonal belt, while the other lies approximately in the plane defined by the Re(7)C(8)C(9)B-(10) face, transoid to the facial carbon C(8) (C(8)−Re(7)−P(1) 158.36(12)°). The carbonyl ligand is disposed transoid to the cage B(10) vertex (C(1)−Re(7)−B(10) 161.82(19)°) and is essentially linear (Re(7)−C(1)−O(1) 177.6(4)°).

Routine PSE (polyhedral skeletal electron) counting procedures,[2,3] with a d^7 ML_3 $Re(CO)(PPh_3)_2$ vertex contributing 1 PSE, yield a structure prediction of $n + 1$ *closo*. The observed polyhedral distortion, however, leads to the *isonido* assignment, contrary to the Wade–Williams formalism. That said, consideration of formal valency leads us to conclude that the complex notionally results from the combination of

(4) (a) For a review of the electrochemistry of many prototypical metallacarboranes and carboranes see: Morris, J. H.; Gysling, H. J.; Reed, D. *Chem. Rev.* **1985**, *85*, 51. (b) Geiger, W. E., Jr.; Smith, D. E. *J. Electroanal. Chem.* **1974**, *50*, 31.

(5) (a) Hawthorne, M. F.; Zink, J. I.; Skelton, J. M.; Bayer, M. J.; Liu, C.; Livshits, E.; Baer, R.; Neuhauser, D. *Science* **2004**, *303*, 1849. (b) Crespo, O.; Gimeno, M. C.; Jones, P. G.; Laguna, A.; López-de-Luzuriaga, J. M.; Monge, M.; Pérez, J. L.; Ramón, M. A. *Inorg. Chem.* **2003**, *42*, 2061. (c) Bitner, T. W.; Wedge, T. J.; Hawthorne, M. F.; Zink, J. I. *Inorg. Chem.* **2001**, *40*, 5428. (d) Hong, E.; Jang, H.; Kim, Y.; Jeoung, S. C.; Do, Y. *Adv. Mater.* **2001**, *13*, 1094. (e) Calhorda, M. J.; Crespo, O.; Gimeno, M. C.; Jones, P. G.; Laguna, A.; López-de-Luzuriaga, J. M.; Perez, J. L.; Ramon, M. A.; Veiros, L. F. *Inorg. Chem.* **2000**, *39*, 4280.

(6) (a) Fischer, M. J.; Jelliss, P. A.; Phifer, L. M.; Rath, N. P. *Inorg. Chim. Acta* **2005**, *358*, 1531. (b) Fischer, M. J.; Jelliss, P. A.; Orlando, J. H.; Phifer, L. M.; Rath, N. P. *J. Lumin.* **2005**, *114*, 60. (c) Jelliss, P. A.; Mason, J.; Nazzoli, J. M.; Orlando, J. H.; Vinson, A. *Inorg. Chem.* **2006**, *45*, 370.

(7) (a) Ellis, D. D.; Jeffery, J. C.; Jelliss, P. A.; Kautz, J. A.; Stone, F. G. A. *Inorg. Chem.* **2001**, *40*, 2041. (b) Ellis, D. D.; Jelliss, P. A.; Stone, F. G. A. *Organometallics* **1999**, *18*, 4982. (c) Blandford, I.; Jeffery, J. C.; Jelliss, P. A.; Stone, F. G. A. *Organometallics* **1998**, *17*, 1402.

Chart 1. *Isonido*-, *Closo*-, and *Hypercloso*-MC_xB_{9-x} ($x = 0-2$) Cage Frameworks.[a]

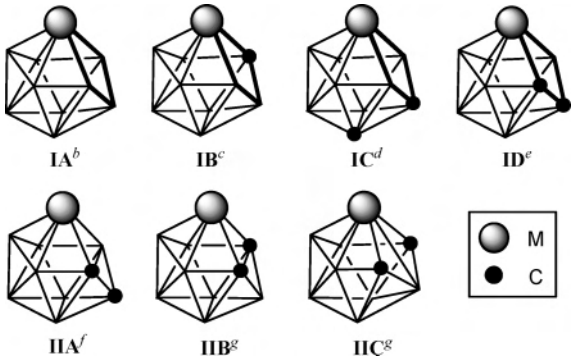

[a] Boron vertexes are unmarked, and open *isonido* faces are emphasized with bold lines. [b]Reference 8. [c]Reference 9. [d]Reference 10. [e]This work. [f]Not reported to date. [g]Reference 13.

a *nido*-$C_2B_7H_9^{2-}$ ligand with a $[Re^{III}(H)L_3]^{2+}$ metal−ligand fragment. The intense color of the compound is certainly commensurate with a Re^{III} formulation; simple $Re^{I}C_xB_{11-x}$ ($x = 1, 2$) complexes are well-known to be weakly colored or more usually colorless.[1a,7]

The pentadecahedral *isonido* cage architecture, although rarely reported in the literature, has been established for metallaborane (**IA**),[8] metallamonocarborane (**IB**),[9] and metalladicarborane (**IC**)[10] systems of Ru, Os, Ir, and Pt only (Chart 1). A 10-vertex *isonido* rhodathiaborane has also been recently described by Barton and co-workers.[11] These structures have also been invoked in *closo*−*isocloso* transformations of MC_xB_{9-x} ($x = 0-2$) systems.[12] Complex **2** is the first rhenium, pre-platinum-block MC_2B_7 metalladicarborane in the *isonido* class **ID** and notably comprises a configuration with both carbon vertexes in the quadrilateral face. Interestingly, the parent *closo* species, **IIA**, has not yet been reported, although Hawthorne and co-workers have characterized *closo* and *hypercloso* ruthenacarborane species with structures **IIB** and **IIC**, respectively.[13] Stone and co-workers have disclosed the synthesis of the only other *isonido* metalladicarborane, [5,8-Me_2-7,7-$(PEt_3)_2$-*isonido*-7,5,8-$PtC_2B_7H_7$], produced as the isomer type **IC** with one facial carbon vertex.[10] Although arguably the first *isonido* species to be reported, it has not been credited as such. Just two other *isonido*-MC_xB_{9-x} ($x = 0-2$) structures share the phenomenon of bridging endopolyhedral hydrogens, those of [7,7,9-$(PPh_3)_3$-*isonido*-7-IrB_9H_{10}] and [3-Cl-7,9-$(PPh_3)_2$-7,10-μ-(*o*-$Ph_2PC_6H_4$)-*isonido*-7-IrB_9H_{10}] (both metallaborane type **IA**), which tentatively bear them on opposite Ir−B and B−B faces of the quadrilateral aperture.[8b]

Complex **2** was also characterized by IR, NMR, and UV−vis spectroscopies and by microanalysis (see Experimental Section). Thus, a single ν_{max}(CO) absorption was observed at 1928 cm^{-1}, suggesting CO loss upon reaction with PPh_3. An $^1H\{^{11}B\}$ NMR spectrum verified the presence of two PPh_3 ligands with a customary multiplet integrating 30:7:2:1 with the terminal cage B−H and C−H proton, and *endo*-H proton singlets, respectively. The *endo*-H atom was identified by its broad, metal-perturbed shift at δ −7.61, which despite this broadening, showed doublet coupling $^2J_{HH} = 14$ Hz. This was matched by the appearance of a second doublet in the same spectrum, also with $^2J_{HH} = 14$ Hz at δ 1.67, identified as one of the terminal cage B−H protons. The observation of seven and two distinct signals for the terminal cage B−H and C−H hydrogens, respectively, reflects the high degree of asymmetry observed in the above-described crystal structure. As a further consequence of this, the $^{31}P\{^1H\}$ NMR spectrum revealed two distinct resonances (δ 12.0 and 12.5) and the $^{11}B\{^1H\}$ spectrum seven resonances. However, the latter spectrum was conspicuous in that its most downfield signal was extraordinarily deshielded (δ 86.7) relative to the remaining range of signals (δ −3.2 to −26.4). This was at first misleading because such an isolated displacement is often indicative of exopolyhedral substitution for hydrogen at a boron vertex.[14] This finding was initially all the more puzzling because the aforementioned complex reported by Stone, [5,8-Me_2-7,7-$(PEt_3)_2$-*isonido*-7,5,8-$PtC_2B_7H_7$], displayed ^{11}B resonances in a much narrower range (δ 28.4 to −1.6). However, a fully coupled ^{11}B NMR spectrum of complex **2** showed $^1J_{HB} > 100$ Hz for all resonances, indicating a terminal hydrogen atom remains fully engaged at this vertex. Furthermore, ^{11}B NMR spectra of several *isonido*-MC_2B_8 species (M = Ru, Os) have shown similarly wide ^{11}B chemical shift ranges (ca. δ 62 to −42 on average) with one particularly deshielded signal.[15] Although an additional vertex is present compared with complex **2**, the comparison may be more suitable because they too possess a quadrilateral *isonido*-$\overline{MCCB}$ face, i.e., 1 boron + 2 carbon facial vertexes. The full ^{11}B chemical shift range for complex **2** ($\Delta\delta = 113$) appears to be the largest yet observed for a metalla(car)borane complex. Because of limited solubility in addition to some very short T_1 relaxation constants for the identified ^{11}B resonances (0.69−2.30 ms), suitable 2D $^{11}B\{^1H\}-^{11}B\{^1H\}$ COSY and $^1H-^{11}B\{^1H\}$ HETCOR NMR spectra could not be obtained. However, ^1H NMR spectra measured with systematically selective ^{11}B decoupling permitted correlation of the cage ^1H resonances with those of the ^{11}B NMR spectrum (Scheme 2). These experiments notably linked the *endo*-H(7) proton to the ^{11}B resonance at δ −4.3. Furthermore, a 2D $^1H\{^{11}B\}-^1H\{^{11}B\}$ COSY NMR spectrum (Figure 2) of complex **2** revealed a strong correlation between resonances at δ −7.61 (the *endo*-H(7) proton) with the signal at δ 1.67, which correlates with the ^{11}B resonance at δ −4.3. Because only the facial B(10) vertex should display any coupling to both a terminal and the *endo*-bridging proton, this ^{11}B resonance (δ −4.3) may

(8) (a) Bould, J.; Brint, P.; Kennedy, J. D.; Thornton-Pett, M. *Acta Crystallogr.* **1990**, *C46*, 1010. (b) Bould, J.; Kennedy, J. D.; Thornton-Pett, M. *J. Chem. Soc., Dalton Trans.* **1992**, 563.
(9) Crook, J. E.; Greenwood, N. N.; Kennedy, J. D.; McDonald, W. S. *J. Chem. Soc., Chem. Commun.* **1981**, 933.
(10) Green, M.; Spencer, J. L.; Stone, F. G. A.; Welch, A. J. *J. Chem. Soc., Chem. Commun.* **1974**, 571.
(11) Volkov, O.; Rath, N. P.; Barton, L. *Organometallics* **2003**, *22*, 2548.
(12) King, R. B. *Inorg. Chem.* **1999**, *38*, 5151.
(13) Jung, C. W.; Baker, R. T.; Knobler, C. B.; Hawthorne, M. F. *J. Am. Chem. Soc.* **1980**, *102*, 5782.
(14) Brew, S. A.; Stone, F. G. A. *Adv. Organomet. Chem.* **1993**, *35*, 135.
(15) Brown, M.; Grüner, B.; Štíbr, B.; Fontaine, X. L. R.; Thornton-Pett, M.; Kennedy, J. D. *J. Organomet. Chem.* **2000**, *614*−*615*, 269.

Scheme 2. Correlations through Selectively Decoupled $^1H\{^{11}B\}$ NMR Spectra (Solid Lines) and a $^1H\{^{11}B\}-^1H\{^{11}B\}$ COSY NMR Spectrum (Dotted Line)[a]

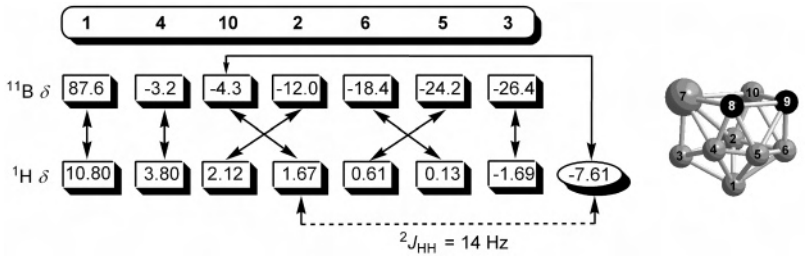

[a] Correlations between terminal-only protons are not indicated. Boron vertex numbers from the cage structure (right) are shown along the top line.

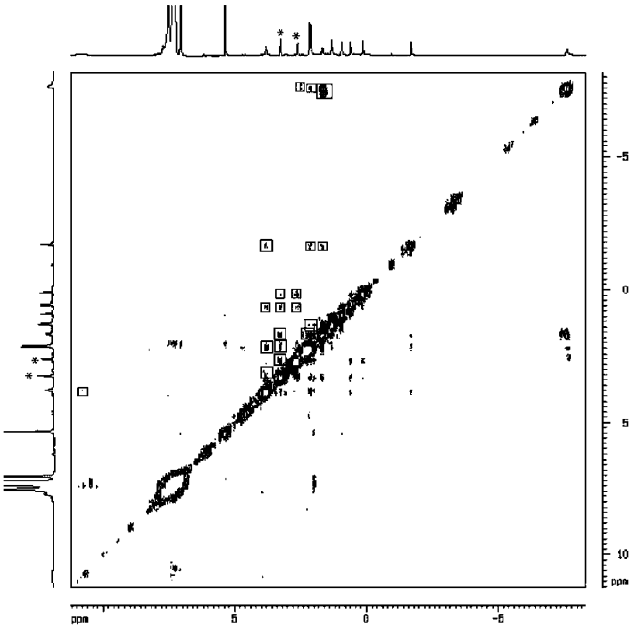

Figure 2. 2D $^1H\{^{11}B\}-^1H\{^{11}B\}$ COSY NMR spectrum of complex **2** in CD_2Cl_2. Off-diagonal correlations indicated on one side by boxes, cage CH's denoted by an asterisk.

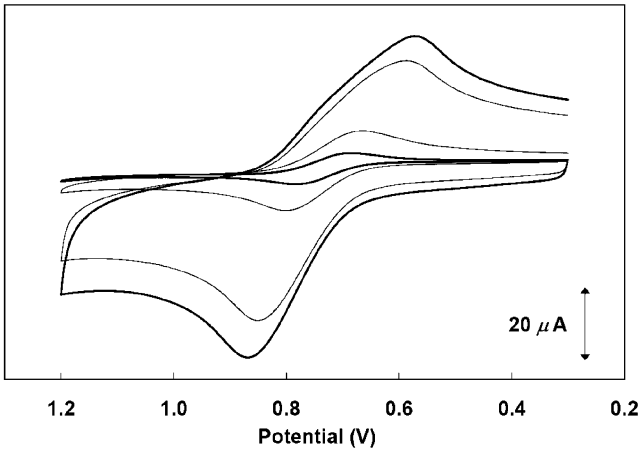

Figure 3. Cyclic voltammograms for a CH_2Cl_2 solution (0.68 mM) of complex **2** at scan rates 0.02, 0.10, 1.00, and 1.50 V s^{-1} relative to Ag/$AgNO_3$ (MeCN, 10 mM).

unequivocally be assigned to B(10). The remaining off-diagonal peaks in the 2D $^1H\{^{11}B\}-^1H\{^{11}B\}$ COSY NMR spectrum permitted reasonably confident assignment of the other ^{11}B chemical shifts, as indicated in Scheme 2.

CV (cyclic voltammetry) measurements (Figure 3) with CH_2Cl_2 solutions of complex **2** revealed a reversible one-electron oxidation ($E_{1/2}$ = 0.67 V, ΔE_p = 82 mV (0.02 V s^{-1}) vs ferrocene, ΔE_p = 90 mV (0.02 V s^{-1})). Reversibility was confirmed by DPV (differential pulse voltammetry) scans in both directions (Supporting Information), which gave an integrated charge ratio, q_{pa}/q_{pc} = 1.07 in addition to the peak current ratio at the slowest scan rate measured (0.02 V s^{-1}), i_{pa}/i_{pc} = 1.02. Diffusion control was established in both scanning directions with linear $\nu^{1/2} - |i_p|$ plots (Supporting Information). The peak current ratios are observed to increase gradually with increasing scan rate to i_{pa}/i_{pc} = 1.39 at 1.50 V s^{-1}, suggestive of an $\vec{\mathbf{E}}C_{rev}$ mechanism at minimum. Supporting this assertion, the oxidative peak displacement, ΔE_{pa} = 55 mV $decade^{-1}$ increase in scan rate, close to the theoretical 59 mV expected for a reversible chemical reaction following a one-electron redox event.[16]

Closer inspection of the CV traces, however, reveals distortion of the reductive wave at the higher scan rates so that an $\vec{\mathbf{E}}C_{rev}\overleftarrow{\mathbf{E}}$ square scheme mechanism may be more appropriate. Given the *isocloso* rhenacarborane system under scrutiny, a logical chemical reaction would result from the expected plasticity of the cage to yield a formally *closo* architecture, accomplished by the formation of an additional connectivity between Re(7) and C(9) to give a type **IIA** structure (Chart 1). From the perspective of PSE counting rules, where one would conclude such a formal *nido* structure for complex **2** (*isonido* or otherwise) is anomalously electron deficient, this outcome is the likely mitigation of what could be viewed as even further loss of PSE. One presumption made in this mechanism is that the bridging hydrogen atom H(7) is displaced from the closing *nido* face to become a terminal hydride ligand on the Re atom, with this consequence perhaps even facilitating the redox-driven deformation. Such a conclusion is borne out of the apparent inability of endopolyhedral hydrogen atoms to bridge deltahedral (3-vertex) faces in stable carboranes. Thus, a likely scenario for the square scheme mechanism is given in Scheme 3 and is supported by digital CV simulation studies (Supporting Information).

Despite the mechanistic complexity, the same solution was shown to be stable to repeated potential cycling and the CV scan fully reproducible over a period of several hours. If the redox process is metal centered, this would represent an unusual reversible $Re^{IV/III}$ event for such a carbonyl-bearing

(16) (a) Bard, A. J.; Faulkner, L. R. *Electrochemical Methods: Fundamentals and Applications*; Wiley: New York, 2000. (b) Astruc, D. *Electron Transfer and Radical Processes in Transition-Metal Chemistry*; VCH: New York, 1995.

Scheme 3. Square Scheme ($\vec{E}C_{rev}\vec{E}$) Mechanism in the Oxidation of Complex **2**[a]

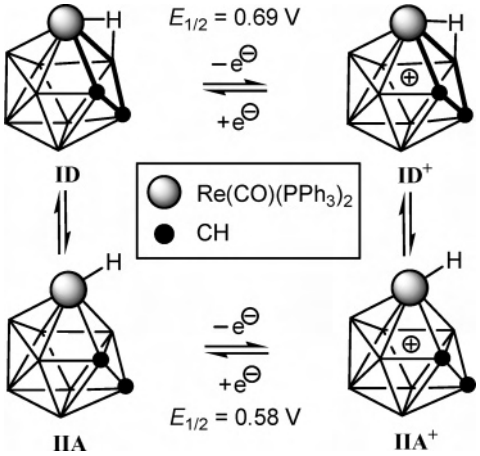

[a] Potentials quoted relative to ferrocene.

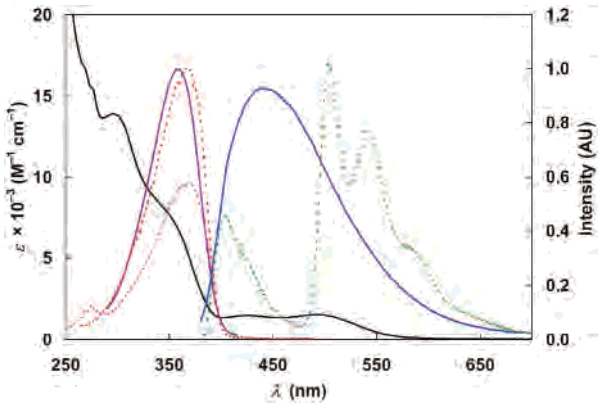

Figure 4. UV−vis spectrum of complex **2** in CH_2Cl_2 (solid black line) (left ordinate). Photoluminescence spectra in CH_2Cl_2 (50 μM, 298 K): excitation (λ_{em} = 442 nm) (solid magenta line); emission (λ_{ex} = 360 nm) (solid blue line). Photoluminescence spectra in MeTHF (50 μM, 77 K): excitation (λ_{em} = 504 nm) (dotted red line); excitation (λ_{em} = 405 nm) (dotted pink line); emission (λ_{ex} = 368 nm) (dotted green line). Photoluminescence intensity (right ordinate) normalized relative to maximum excitation intensities.

organometallic complex. Chemical oxidation of CH_2Cl_2 solutions of complex **2** with the ammoniumyl salt [N(*p*-C_6H_4-Br)$_3$][$SbCl_6$] did indeed reveal a clean displacement of the CO stretching absorption to ν_{max}(CO) = 2039 cm^{-1}. A change of $\Delta\nu$ = +111 cm^{-1} is consistent with a metal-centered oxidation.[6c,17] Solutions of **2**$^+$, however, appear to not be stable to isolation procedures, with IR spectra showing quantitative reformation of neutral complex **2** over a period of several hours.

Perhaps even more uncharacteristic in this field of organometallic chemistry is the ambient-temperature luminescence of CH_2Cl_2 solutions of complex **2** (Figure 4). Thus, complex **2** strongly emits light at λ_{em} = 442 nm (Φ = 0.012) with excitation at λ_{ex} = 360 nm (Stokes shift = 5330 cm^{-1}) with no irregular concentration dependence. Photoluminescence results were reproducible from multiple batches of pure, chromatographed complex **2**, as ascertained by spectroscopic and microanalytical data. Although λ_{em} corresponds

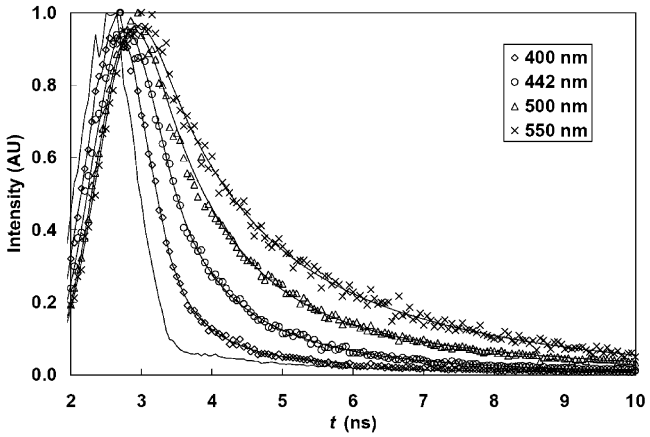

Figure 5. Fluorescence decay for sampled emission wavelengths from a solution of complex **2** in CH_2Cl_2 at 298 K, λ_{ex} = 360 nm. Curve fits are shown in addition to instrument response function (solid lines).

to blue emission, solutions of **2** characteristically luminesce turquoise-blue when placed over a hand-held UV lamp with a long-wave source, reflecting the broadness of the emission (peakwidth-at-half-height = 5900 cm^{-1}). Time-based experiments showed no variation of emission intensity over a period of 400 s, confirming that the emissive species is not a dissociative photoproduct and that the lumophore is in fact optically stable. Thus, free PPh_3, which actually luminesces much more weakly at $\lambda_{em} \approx$ 475 nm (Φ = 0.003 in benzene at 298 K),[18] is not the species responsible for emission in this case. This was also confirmed by careful NMR analysis, which showed no decomposition of complex **2** upon prolonged photolysis at λ_{ex} = 360 nm and the absence of free PPh_3.

Comparison of the excitation/emission peak shapes, even on an energy scale, reveals a perceptible asymmetry. Thus, the emissive excited-state species may not share the same ground-state nuclear arrangement of the parent complex, which is feasible given the redox characteristics of complex **2** discussed above and the d−d phosphorescence observed for the complex [3-CO-3,3-{κ^2-$Me_2N(CH_2)_2NMe_2$}-*closo*-3,1,2-$RuC_2B_9H_{11}$].[6c] This phenomenon, however, may necessarily be the consequence of the mixing of multiple excited states of complex **2**. This was evidenced by decay lifetime measurements in CH_2Cl_2 measured at ambient temperatures (Figure 5, Table 1). Sampling at a variety of wavelengths along the emission profile revealed monoexponential, very short-lived fluorescence at the high-energy extreme (τ = 0.39 ns at λ_{em} = 400 nm), with biexponential decay at the emission peak (τ_1 = 0.44 ns (74%) and τ_2 = 1.1 ns (26%) at λ_{em} = 442 nm). At lower energies (λ_{em} = 500 and 560 nm), the shorter lifetime component (≥71%) approaches 1 ns along with a minor contribution (≤29%) from super-3.0 ns decay. Clearly, all emitting states are fluorescent with a net result that is apparent from Figure 5: the emission tail is evidently longer-lived than at the high-energy extreme.

Measurements in MeTHF (2-methyltetrahydrofuran) glass at 77 K (Figure 4) resulted in two distinct structured

(17) (a) Connelly, N. G.; Johnson, G. A. *J. Organomet. Chem.* **1974**, *77*, 341. (b) Carriedo, G. A.; Riera, V.; Connelly, N. G.; Raven, S. J. *J. Chem. Soc., Dalton Trans.* **1987**, 1769.

(18) (a) Segers, D. P.; DeArmond, M. K.; Grutsch, P. A.; Kutal, C. *Inorg. Chem.* **1984**, *23*, 2874. (b) Changenet, P.; Plaza, P.; Martin, M. M.; Meyer, Y. H.; Rettig, W. *Chem. Phys.* **1997**, *221*, 311.

Table 1. Decay Lifetime Analysis for Complex **2**

T/K (solvent)	λ_{em}/nm[a]	τ_1/ns (a_1/%)[b]	τ_2/ns (a_2/%)[b]	χ^2 [c]
298 (CH_2Cl_2)	400	0.39 (100)	–	1.37
	442[d]	0.44 (74)	1.1 (26)	1.29
	500	0.81 (89)	3.2 (11)	1.22
	560	0.86 (71)	3.0 (29)	0.97
77 (MeTHF)	405	0.18 (92)	0.74 (8)	0.97
	504	0.40 (88)	4.7 (12)	0.99
	543	0.36 (77)	4.3 (23)	1.39
	585	0.49 (72)	5.1 (28)	0.82

[a] Emission wavelength for decay sampling. Excitation, $\lambda_{ex} = 360$ (298 K) and 368 nm (77 K). [b] Lifetime(s) τ_n with percent contribution, a_n, shown in parentheses. [c] χ^2 (Marquardt−Levenberg) fit. [d] Emission peak, $\Phi_{442} = 0.012$.

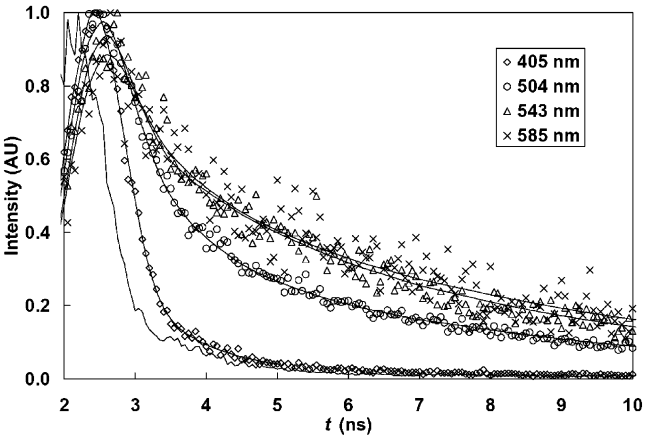

Figure 6. Fluorescence decay for sampled emission wavelengths from a solution of complex **2** in MeTHF at 77 K, $\lambda_{ex} = 368$ nm. Curve fits are shown in addition to instrument response function (solid lines).

emissions at $\lambda_{em} = 405$ and 504 nm. The latter (Stokes shift = 7260 cm^{-1}) comprises obvious vibrational fine structure ($\Delta\nu = 1425$ cm^{-1}, Huang−Rhys factor, $I_{0,1}/I_{0,0} = 0.75$), while the former (Stokes shift = 2470 cm^{-1}) shows less resolved structure ($\Delta\nu \approx 1400$ cm^{-1}). It should be noted that, while the emission spectra at 298 and 77 K are radically different, the corresponding excitation spectra differ only slightly in λ_{ex} ($\Delta\lambda = 8$ nm) and not at all in line shape. Moreover, the excitation appears to correspond with a moderately strong absorption shoulder ($\lambda_{max} = 355$ nm, $\epsilon = 7200$ M^{-1} cm^{-1}) in the UV−vis spectrum also measured in CH_2Cl_2 at 298 K (Figure 4) that is solvent independent. Decay lifetime measurements in MeTHF measured at 77 K (Figure 6, Table 1) ruled out any phosphorescent contribution to the lower energy emission especially, despite the moderately large Stokes shift. Thus, the 405 nm violet emission is exceedingly short-lived, and though formally biexponential, is dominated by the $\tau = 0.18$ ns (92%) decay. Sampling of the lower energy green emission reveals somewhat longer biexponential contributions with $\tau = 0.40$ (88%) and 4.7 ns (12%) at $\lambda_{em} = 504$ nm and only slight variation of these parameters at longer wavelength peaks/shoulders at $\lambda_{em} =$ 543 and 585 nm. The longest decay measured (5.1 ns (28%)) in the emission tail is still clearly fluorescent. Nevertheless, the highly structured green emission all but disappeared (89% decrease in integrated intensity) when measurements were carried out with a high concentration (10 mM) of the well-known triplet quencher, anthracene, even at 77 K where translational motion should be highly restricted (Supporting Information). Any 405 nm emission from complex **2** was masked by the strong anthracene luminescence.

An IR spectrum of complex **2** in CH_2Cl_2 does indeed display medium-intensity absorptions at 1430 and 1434 cm^{-1}, which are nominally assigned to aryl C−C *n* stretching modes in the phosphine ligand and tend to be invariant between the free PPh_3 ligand and its coordination compounds.[19] This would thus seem to identify the PPh_3 ligand(s) as a critical component of the lumophore in complex **2**. However, the only report of Re−phosphine luminescence is that of d−d emission from the Re^{I} complexes $[Re(Cl)L_2(CO)_3]$ ($L = PPh_3$, $P(o\text{-}C_6H_4Me)_3$; $L_2 = Et_2P(CH_2)_2PEt_2$),[20] which due to the strength and energy of the excitation, as well as its frozen (77 K) glass behavior described above, is most unlikely to be responsible for the luminescence of complex **2**. What is more, there have been no reports of emission from a complex with a mononuclear Re^{III} center. Indeed, this oxidation state might be considered to be photophysically benign for mononuclear rhenium complexes with only Re^{I} and Re^{VII} centers being acknowledged as established lumophores.[21] The observed 77 and 298 K emissions are nevertheless consistent with metal-perturbed ^{1}IL dual fluorescence (Scheme 4a), with the impact of the metal evident from the Huang−Rhys factor for the longer-wavelength emission, normally >1.0 for pure IL progressions.[22] Specifically $\sigma_{ReP}-\sigma_{PC}$* singlet emission is proposed, where contribution from P−C σ* antibonding orbitals to the excited state is suggested. Given the propensity of these orbitals to also engage with the metal d_π orbitals (as well as P 3d orbitals of course),[23] the total asymmetry of the complex no doubt assists in any relaxation of Laporte selection rules. The P−C σ* component would be consistent with the vibronic structure observed at 77 K in Figure 4 because aryl C−C *n* stretching modes at ca. 1430 cm^{-1} in aryl phosphines (coordinated or uncoordinated) cannot occur independently from P−C bond deformation (Figure 7). The stimulation of these stretching modes by occupation of an orbital with P−C σ* character can thus be readily appreciated.

The excitation for complex **2** ($\lambda_{ex} = 360$ nm) also lies at considerably lower energy than ligand-isolated $\pi-\pi$* or $n-a_\pi$ transitions.[18] The observed emissions are likewise inconsistent with $\sigma-a_\pi$ (Re−P σ-bond → aryl π* orbital) states observed in other luminescent metal−phosphine complexes from the late d block, which show some solvent dependency (especially for the $^3\sigma-a_\pi$ phosphorescence), and

(19) (a) Crayston, J. A.; Davidson, G. *Spectrochim. Acta* **1986**, *42A*, 1311. (b) Deacon, G. B.; Green, J. H. S. *Spectrochim. Acta* **1968**, *24A*, 845. (c) Whiffen, D. H. *J. Chem. Soc.* **1956**, 1350.
(20) Ramsis, M. N. *Monatsh. Chem.* **1993**, *124*, 849.
(21) Vogler, A.; Kunkely, H. *Coord. Chem. Rev.* **2000**, *200−202*, 991.
(22) (a) Miskowski, V. M.; Houlding, V. H. *Inorg. Chem.* **1989**, *28*, 1529. (b) Miskowski, V. M.; Houlding, V. H. *Coord. Chem. Rev.* **1991**, *111*, 145. (c) Miskowski, V. M.; Houlding, V. H.; Che, C.-M.; Wang, Y. *Inorg. Chem.* **1993**, *32*, 2518. (d) Buchner, R.; Cunningham, C. T.; Field, J. S.; Haines, R. J.; McMillin, D. R.; Summerton, G. C. *J. Chem. Soc., Dalton Trans.* **1999**, 711.
(23) (a) Orpen, A. G.; Connelly, N. G. *J. Chem. Soc., Chem. Commun.* **1985**, 1310. (b) Pacchioni, G.; Bagus, P. S. *Inorg. Chem.* **1992**, *31*, 4391. (c) Crabtree, R. H. In *The Organometallic Chemistry of the Transition Metals*; Wiley: New York, 2001; Ch. 4, pp 92−93.

Scheme 4. Energy Level Diagrams for (a) Dual Fluorescence of Complex **2** at 77 K and (b) Fluorescence Quenching by Singlet−Triplet Energy Transfer to Anthracene

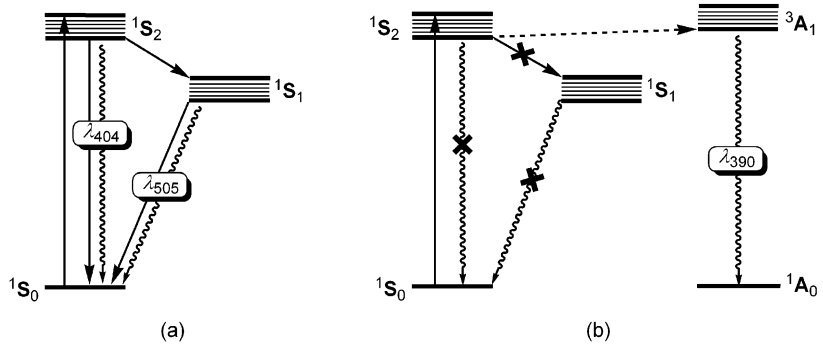

do not display similarly structured emissions, irrespective of temperature.[18a,24] Both absorption and emission spectra for complex **2** are completely solvent-invariant in λ, with the spectra in DMF, for instance, appearing the same as those in Figure 4, suggesting little or no charge transfer. The quenching observed upon the addition of anthracene at 77 K must result from rapid intermolecular singlet−triplet energy transfer ($k_{ET} > 10^9$ s^{-1}) as indicated in Scheme 4b. Efficient diversion of energy from the upper $^1\mathbf{S}_2$ state of complex **2** to the energy-matched anthracene $^3\mathbf{A}_1$ excited state effectively shuts down intersystem crossing to $^1\mathbf{S}_1$, and thus, the dual fluorescence is mostly quenched.

From excitation measurements, it seems that the lower excited state $^1\mathbf{S}_1$ is not directly accessible by absorption from the $^1\mathbf{S}_0$ ground state, as there are no further excitation peaks at lower energy, despite the presence of moderately weak absorptions in the UV−vis spectrum at $\lambda_{max} = 424$ and 493 nm. This would ultimately suggest a small but significant and rapid nondissociative nuclear displacement resulting from the primary excitation at $\lambda_{ex} = 360$ nm. The most likely scenario is a minor adjustment in metal coordination geometry. However, given that the excitation involves displacement of electron density from an orbital directly involved in PSE cage-cluster bonding to an orbital which is not, some cage deformation, namely an *isonido*−*closo* conversion might also be feasible. Such a modification was of course invoked in the redox chemistry of complex **2** (vide supra), and simulation experiments support a rapid structure reassignment, although we cannot say at this point whether it is fast enough to accommodate the fluorescent state observed for complex **2**. We have previously implicated cage deformation in the d−d phosphorescence of [3-CO-3,3-{κ^2-$Me_2N(CH_2)_2NMe_2$}-*closo*-3,1,2-$RuC_2B_9H_{11}$], although this complex displays a much longer decay lifetime (τ = 0.77 ms), albeit at 77 K.[6c] At this point, our inclination is to favor an ancillary role for the carborane cage in the photophysical behavior of **2**, especially given our observation of very similar luminescence characteristics with the recently isolated Re^{III} complex [3-Cl-3-CO-3,3-$(PMe_3)_2$-*closo*-3,1,2-$ReC_2B_9H_{11}$].[25] However, we expect to continue our investigations with the isolation and characterization of further rhenacarborane−phosphine complexes.

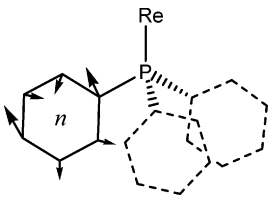

Figure 7. Aryl C−C *n* stretching mode in the PPh_3 ligand. The notation is taken from ref 19c.

Conclusion

Complex **2** has been synthesized and thoroughly characterized by X-ray crystallography and by NMR, IR, and UV−vis spectroscopic analysis, revealing an asymmetric *isonido*-7,8,9-ReC_2B_7 structure, comprising a tripodal $Re(CO)(PPh_3)_2$ vertex. Electrochemical measurements in CH_2Cl_2 solution have revealed a reversible one-electron square scheme with an associated *isonido*−*closo* transformation, which is not altogether surprising from the viewpoint of metallacarborane cage PSE counting. The strong ambient temperature fluorescence, on the other hand, was unexpected given this class of complex and especially the oxidation state of the metal (Re^{III}). The short fluorescent lifetimes, with major components in the sub-nanosecond regime, are no doubt a major contributor to the observed respectable quantum yield in solution at room temperature. At present, the involvement of the carborane ligand with the lumophore appears to be trivial, but with the opening of this avenue of investigation, it may be prudent at some point to investigate previously reported metallacarborane complexes for potentially interesting photophysical behavior. For our part, we continue to probe this and other related rhenacarborane phosphine complexes for their candidacy as redox and dye mediators in biofuel and photovoltaic cells, respectively.

Experimental Section

General Considerations. Solvents (CH_2Cl_2, DMF, hexanes, MeCN, THF, MeTHF) were distilled over appropriate drying agents under argon prior to use. All reactions were carried out under a dry, oxygen-free argon atmosphere using Schlenk line and glovebox techniques. Complex **1** was prepared using the literature method.[6a] The reagent PPh_3 was purchased from Aldrich and used as received.

(24) (a) Kunkely, H.; Vogler, A. *J. Am. Chem. Soc.* **1995**, *117*, 540. (b) Kunkely, H.; Vogler, A. *Coord. Chem. Rev.* **2002**, *230*, 243.
(25) Buckner, S. W.; Fischer, M. J.; Jelliss, P. A.; Minteer, S. M.; Rath, N. P. Unpublished results. See Supporting Information for preliminary data for this complex.

Instrumentation. All solution measurements were made at 298 K unless otherwise stated. IR measurements were made using solution cells in a Perkin-Elmer RX-I FTIR spectrometer. NMR measurements were recorded using a Varian Gemini 300 MHz spectrometer, ^{1}H (300.0 MHz); ^{13}C (75.4 MHz);^{11}B (96.3 MHz); ^{31}P (121.4 MHz), or a Bruker ARX 500 MHz spectrometer, ^{1}H (500.1 MHz); ^{13}C (125.6 MHz);^{11}B (160.5 MHz); ^{31}P (202.5 MHz). Selective decoupling experiments and 2D spectra were exclusively measured on the latter instrument. Electrochemical experiments were performed with a CH Instruments CHI620B electrochemical analyzer. All potentials were recorded relative to an $Ag/AgNO_3$ (MeCN, 10 mM) reference electrode at 298 K and quoted relative to an internal ferrocene standard. All solutions were studied in a three-electrode cell under Ar in distilled, deoxygenated solvents and contained 0.1 M $[NBu^n_4][PF_6]$ as supporting electrolyte. All CV and DPV measurements were made on a glassy carbon disk working electrode with a surface area of 7.07 mm^2, which was frequently polished, rinsed, and dried between measurements. The Pt wire counter electrode was precleaned by soaking in concentrated HNO_3, rinsed with distilled water, and then flame-dried. Cyclic voltammograms were run both with initial positive and negative scan polarities, and showed little variation with this parameter. Digital simulations were carried out using DigiElch.[26] UV−vis spectral measurements (800 → 220 nm) were made with a Shimadzu 2530 UV−visible absorption spectrophotometer. Photoluminescence measurements were made with a Photon Technologies QM4 fluorescence spectrophotometer with a Xe arc lamp light source and digital PMT detector. Emission and reference source gain excitation corrections were applied to all steady-state data. Slit widths were typically set at 5 nm. Appropriate cutoff filters were used to eliminate peaks due to solvent Raman-shifted bands and excitation harmonics when possible. Solution samples at ambient temperatures were measured in a quartz sample cuvette with Schlenk attachment to deoxygenate samples. Samples measured at 77 K were degassed and analyzed in a quartz NMR tube with Schlenk attachment and set in quartz-bottomed Dewar flask in an argon-filled sample chamber. The quantum yield was assessed by comparison of integrated peak intensities between those of complex **2** for the full range of emission wavelengths and the singlet emission from deoxygenated 9-cyanoanthracene in hexane, which has $\Phi_{em} = 1.00$. The concentration of the complex **2** solution was adjusted to give an accurately measured absorbance of ca. 0.1 A at λ_{ex}. A standard solution of 9-cyanoanthracene was similarly created and its integrated emission intensity measured using an optical density (OD1) filter at the emission monochromator entrance at consistently fixed slit widths for all measurements. Quantum yields were then calculated according to

$$\Phi_{em} = \frac{I_{int,x}/f_x}{(I_{int,c}/f_c) \times 100}$$

where I_{int} = integrated intensity, f = fraction of light absorbed for a solution of complex **2** (x) and of 9-cyanoanthracene (c). Integrated emission intensities, I_{int}, were thus corrected for self-absorption using transmission data parameters from the UV−vis absorption spectra over the width of the emission band. Accurate fluorescence decays from compound **2** were measured with a PTI model TM-3/2005 lifetime fluorescence spectrophotometer. The instrument employed a PTI GL-330 pulsed nitrogen laser pumping a PTI GL-302 tunable dye laser as an excitation source and a proprietary stroboscopic detection system with an R928 photomultiplier. The decays were analyzed with a PTI FeliX32 advanced analysis package utilizing a discrete multiexponential fitting function and iterative reconvolution.

Synthesis of [7,10-μ-H-7-CO-7,7-(PPh$_3$)$_2$-*isonido*-7,8,9-ReC$_2$B$_7$H$_9$]. Compound **1** (0.10 g, 0.20 mmol) and PPh_3 (0.16 g, 0.59 mmol) were combined in a three-necked flask fitted with a condenser, which is in turn connected to an Ar/vacuum Schlenk line. The reactants were dissolved in dry distilled THF (30 mL) and heated to reflux for 24 h. After the mixture cooled to room temperature, solvent was removed in vacuo. The residue was dissolved in CH_2Cl_2/hexanes (10 mL, 1:1) and chromatographed on alumina (Brockmann IV) at −25 °C. Elution with the same solvent mixture removed an intense orange-red fraction. Solvent was reduced in volume to 2 mL and hexanes added (5 mL) to afford bright orange-red microcrystals of **2** (0.03 g, 18%), which were washed with hexanes (3 × 20 mL) and dried in vacuo. X-ray-quality crystals were grown from a CH_2Cl_2 solution of **2** layered with hexanes. A second rhenacarborane−carbonyl product was eluted from the column using neat CH_2Cl_2 but has not yet been identified. Data for **2** (298 K): IR (CH_2Cl_2) (cm^{-1}) ν_{max}(BH) 2550m, ν_{max}(CO) 1928s, ν_{max}(CC-*n*) 1430m, 1434m; ^{1}H{^{11}B} NMR (CD_2Cl_2) δ 7.73−7.04 (m, 30 H, Ph), 10.80, 3.80, 2.12, 1.67*, 0.61, 0.13, −1.69 (s × 7, 7 H, cage BH, * $^{2}J_{H^7H^{10}} = 14$), 3.27, 2.64 (s × 2, 2 H, cage CH), −7.61 (d br, 1 H, *endo*-H, $^{2}J_{H^7H^{10}} = 14$); ^{13}C{^{1}H} NMR (CD_2Cl_2) δ 208.8 (CO), 134.5, 134.2 (d × 2, C^i(Ph), $^{1}J_{PC}$ = 47, 47), 133.6, 133.5 (d × 2, C^o(Ph), $^{2}J_{PC}$ = 11, 10), 135.8, 135.2 (d × 2, C^p(Ph), $^{4}J_{PC}$ = 2, 2), 128.2, 127.7 (d × 2, C^m(Ph), $^{3}J_{PC}$ = 10, 9), 45.5, 39.5 (br × 2, cage C); ^{31}P{^{1}H} NMR (CD_2Cl_2) δ 12.5, 12.0 (s × 2); ^{11}B{^{1}H} NMR (CD_2Cl_2) δ (T_1) 86.7 (0.69 ± 0.03 ms), −2.8 (1.20 ± 0.08 ms), −4.0 (2.30 ± 0.08 ms), −11.9 (1.20 ± 0.06 ms), −18.3 (1.14 ± 0.04 ms), −24.2 (1.10 ± 0.06 ms), −26.4 (1.21 ± 0.05 ms) (s × 7); UV−vis. (CH_2Cl_2) λ_{max} (nm) ($\epsilon \times 10^{-3}$ (M^{-1} cm^{-1})) 266sh (17.3), 276sh (16.0), 297 (13.9), 355sh (7.2), 424 (1.5), 493 (1.5); Anal. Calcd for $C_{39}H_{40}B_7OP_2Re$: C, 55.2; H, 4.8. Found: C, 54.8; H, 5.0.

X-ray Crystallography. A crystal of **2** was mounted onto a glass fiber in a random orientation. Preliminary examination and data collection were performed using a Siemens SMART charge-coupled device (CCD) detector system single-crystal X-ray diffractometer equipped with a sealed-tube X-ray source using graphite-monochromated Mo Kα radiation (λ = 0.71073 Å). Preliminary unit cell constants were determined with a set of 45 narrow-frame scans (0.3° in ω). A total of 4026 frames of intensity data were collected at a crystal-to-detector distance of 4.91 cm. The double-pass method of scanning was used to reduce noise. The collected frames were integrated using an orientation matrix determined from the narrow-frame scans. The SMART software package was used for data collection, and SAINT[27] was used for frame integration. Analysis of the integrated data did not show any decay. Final cell constants were determined by a global refinement of the *x*, *y*, *z* centroids of thresholded reflections from the entire dataset. Absorption corrections were applied to the data using equivalent reflections (SADABS).[28] The SHELX-97[29] software package was used for structure solutions (by direct methods) and refinement. Full-matrix least-squares refinement was carried out by minimizing $\sum w(F_o^2 - F_c^2)^2$. The non-hydrogen atoms were refined anisotropically to convergence. Noncage hydrogen atoms were included in calculated positions and treated using appropriate riding models. Cage

(26) Rudolph, M. *DigiElch* ver. 2.0; Friedrich-Schiller-Universität: Jena, Germany, 2005.

(27) *SAINT*; Bruker Analytical X-ray: Madison, WI, 2002.
(28) Blessing, R. H. *Acta Crystallogr.* **1995**, *A51*, 33.
(29) Sheldrick, G. M. *SHELX-97*; University of Göttingen: Göttingen, Germany, 1997.

Table 2. Crystallographic Data for Complex **2**

empirical formula	$C_{39}H_{40}B_7OP_2Re$
fw	848.52
cryst dimens (mm)	0.18 × 0.15 × 0.13
cryst color, shape	red, rectangular prism
cryst syst, space group	monoclinic, $P2_1/c$
a (Å)	10.2488(3)
b (Å)	21.7109(7)
c (Å)	16.2333(5)
β (deg)	98.594(2)
V (Å^3)	3571.53(19)
Z	4
D_{calcd} (g cm^{-3})	1.578
μ(Mo Kα) (mm^{-1})	3.525
T (K)	165(2)
θ range (deg)	1.58−28.00
reflns collcd	85321
indept reflns (R_{int})	8626 (0.065)
wR2, R1[a] ($I > 2\sigma(I)$)	0.0720, 0.0432
wR2, R1[a] (all data)	0.0749, 0.0582
GOF on F^2	1.257
largest diff. peak and hole (e Å^{-3})	1.613, −2.723

[a] Refinement was block full-matrix least-squares on all F^2 data: wR2 = $[\sum\{w(F_o^2 - F_c^2)^2\}/\sum w(F_o^2)^2]^{1/2}$ where $w^{-1} = \sigma^2(F_o^2)$. The value R1 = $\sum||F_o| - |F_c||/\sum|F_o|$.

hydrogens, including the endopolyhedral hydrogen H(7), were located from the difference Fourier map and included in the final refinement. The structure refinement parameters are given in Table 2, and selected bond angles and distances are given in the legend for Figure 1. A complete list of positional and isotropic displacement coefficients for the hydrogen atoms, anisotropic displacement coefficients for the non-hydrogen atoms, and bond distances and angles are available in CIF format as Supporting Information. CCDC 288357 also contains the supplementary crystallographic data for this paper. These data can be obtained free of charge from The Cambridge Crystallographic Data Centre via www.ccdc.cam.ac.uk/data_request/cif.

Acknowledgment. This material is based upon work funded in part by the U.S. Government. Research Corporation (Cottrell Grant No. CC5748) is also acknowledged for the purchase of the fluorescence spectrophotometer. We thank Prof. Lawrence Barton (UMSL) for helpful discussions.

Supporting Information Available: Further electrochemical measurement and analysis of **2** (DPVs, $\nu^{1/2} - |i_p|$ plots, CV digital simulation details). Photoluminescence spectrum of **2** with anthracene quenching. Tables of crystallographic data, including fractional coordinates, bond lengths, and angles, anisotropic displacement parameters, and hydrogen atom coordinates of **2** in CIF file format. This material is available free of charge via the Internet at http://pubs.acs.org.IC061071N

IC061071N